RESOURCE
https://doi.org/10.1038/s41593-018-0187-0

nature neuroscience

Cell-specific histone modification maps in the human frontal lobe link schizophrenia risk to the neuronal epigenome

Kiran Girdhar[1,11], Gabriel E. Hoffman[1,11*], Yan Jiang[2], Leanne Brown[2], Marija Kundakovic[2,3], Mads E. Hauberg[4,5], Nancy J. Francoeur[1], Ying-chih Wang[1], Hardik Shah[1], David H. Kavanagh[1], Elizabeth Zharovsky[2], Rivka Jacobov[2], Jennifer R. Wiseman[2], Royce Park[2], Jessica S. Johnson[1], Bibi S. Kassim[2], Laura Sloofman[1], Eugenio Mattei[6], Zhiping Weng[6], Solveig K. Sieberts[7], Mette A. Peters[7], Brent T. Harris[8,9], Barbara K. Lipska[9], Pamela Sklar[1,2], Panos Roussos[1,2,10*] and Schahram Akbarian[2*]

Risk variants for schizophrenia affect more than 100 genomic loci, yet cell- and tissue-specific roles underlying disease liability remain poorly characterized. We have generated for two cortical areas implicated in psychosis, the dorsolateral prefrontal cortex and anterior cingulate cortex, 157 reference maps from neuronal, neuron-depleted and bulk tissue chromatin for two histone marks associated with active promoters and enhancers, H3-trimethyl-Lys4 (H3K4me3) and H3-acetyl-Lys27 (H3K27ac). Differences between neuronal and neuron-depleted chromatin states were the major axis of variation in histone modification profiles, followed by substantial variability across subjects and cortical areas. Thousands of significant histone quantitative trait loci were identified in neuronal and neuron-depleted samples. Risk variants for schizophrenia, depressive symptoms and neuroticism were significantly over-represented in neuronal H3K4me3 and H3K27ac landscapes. Our Resource, sponsored by PsychENCODE and CommonMind, highlights the critical role of cell-type-specific signatures at regulatory and disease-associated noncoding sequences in the human frontal lobe.

Recent progress in understanding the genetic basis of many psychiatric diseases has identified both rare and common variants responsible for genetic risk[1]. Integrating epigenomics data from disease-relevant cell types and tissues promises to enhance interpretation of these risk variants and the mechanisms by which they confer disease liability[2]. This includes the exploration of noncoding regulatory DNA and its epigenetic variation in mediating the effects of genetic risk variants[2–4]. Thus, the long-term goal of the PsychENCODE[5,6] and CommonMind[7] consortia is to generate a large-scale epigenomics resource for the human brain to serve as a foundation for integrative genomics in psychiatric research[6]. In this regard, nucleosomal histone modifications contribute to genome organization and function, with various histone methylation and acetylation markings, including H3K4me3 and H3K27ac, considered key regulators for active promoters and enhancers and other cis-regulatory noncoding sequences[8]. Importantly, molecular regulators for such types of open-chromatin-associated histone modifications rank as top-scoring biological pathways by genome-wide association in schizophrenia and bipolar disorder[9], further underscoring the importance of fine-mapping histone landscapes in brain. However, only a few publicly available histone datasets and resources exist for the human brain[5,10,11], all of which were created from bulk tissue homogenate. These tissue-homogenate-based resources have clearly contributed to a deeper understanding of the genetic risk architecture of common psychiatric disease. However, there is evidence that, even in the context of normal cortical development and aging, vast portions of the neuronal genome show a very different histone modification landscape in comparison to those of the surrounding glia and other non-neuronal cells[12,13]. Unfortunately, the degree to which cell-type- and region-specific epigenomic signatures mediate the influence of genetic risk factors for psychiatric disease remains largely unexplored.

Here we present the largest dataset to date of open-chromatin-associated histone modifications mapped separately in neurons versus the remaining neuron-depleted cell fraction from two higher order brain areas implicated in schizophrenia and other psychiatric diseases[14]: dorsolateral prefrontal cortex (PFC) and anterior cingulate cortex (ACC). Our publicly accessible resource, available at http://psychencode.org/ and https://www.synapse.org/#!Synapse:syn4566010, includes data, results and UCSC browser visualizations for cell-type-specific maps from $N=129$ samples, complemented with another $N=28$ maps from tissue

[1]Department of Genetics and Genomic Sciences, Icahn Institute of Multiscale Biology, Icahn School of Medicine at Mount Sinai, New York, NY, USA. [2]Department of Psychiatry and Friedman Brain Institute, Icahn School of Medicine at Mount Sinai, New York, NY, USA. [3]Department of Biological Sciences, Fordham University, Bronx, NY, USA. [4]iPSYCH, The Lundbeck Foundation Initiative for Integrative Psychiatric Research, Aarhus, Denmark. [5]Department of Biomedicine, Aarhus University, Aarhus, Denmark. [6]Program in Bioinformatics and Integrative Biology, Department of Biochemistry and Molecular Pharmacology, University of Massachusetts Medical School, Worcester, MA, USA. [7]Systems Biology, Sage Bionetworks, Seattle, WA, USA. [8]Department of Neurology, Georgetown University, Washington, DC, USA. [9]Human Brain Collection Core, NIMH, Bethesda, MD, USA. [10]Mental Illness Research, Education, and Clinical Center, James J. Peters VA Medical Center, Bronx, NY, USA. [11]These authors contributed equally: Kiran Girdhar, Gabriel E. Hoffman. *e-mail: gabriel.hoffman@mssm.edu; panagiotis.roussos@mssm.edu; schahram.akbarian@mssm.edu

homogenate from adult control subjects without known neurological or psychiatric disease (Supplementary Table 1). This epigenomics resource provides hitherto unexplored insights into cell- and region-specific histone methylation and acetylation landscapes, including sites with extraordinarily high inter-individual variability. We elucidate the influence of genetic regulation on chromatin state and identify thousands of significant histone quantitative trait loci (hQTLs). We report striking enrichments of risk variants for schizophrenia, educational attainment, neuroticism and depressive symptoms highly specific to neuronal chromatin, thereby critically confirming cell type as a key variable in the neurogenomic architecture of psychiatric disease.

Results

Samples and sequencing. Nuclei were extracted from previously frozen gray matter collected from two frontal lobe areas implicated in higher order processing serving cognition and emotion: the dorsolateral prefrontal cortex (PFC), at the superior frontal gyrus, and the anterior cingulate cortex (ACC), positioned immediately dorsoanterior to the corpus callosum (Fig. 1a, left). Chromatin immunoprecipitation and sequencing (ChIP-seq) with anti-H3K4me3 and anti-H3K27ac antibodies followed by 100-base-pair paired end sequencing was performed for neuronal and non-neuronal nuclei separately after NeuN neuronal marker immunotagging and fluorescence-activated sorting (Fig. 1a, right). NeuN, broadly expressed in the vast majority of cortical excitatory and inhibitory neurons[15], is a prototypical neuronal marker in adult human cortex[16]. We herein refer to the NeuN$^+$ fraction as neuronal and the NeuN$^-$ fraction as neuron-depleted, while acknowledging that each of these two cell types is comprised of many different subpopulations[17]. Performing cell-type-specific ChIP-seq on two brain regions from each of 17 subjects (14 males and 3 females), we generated $N=129$ cell-type-specific libraries ($N=63$ H3K4me3; $N=66$ H3K27ac), as well as $N=28$ tissue-homogenate-based libraries from $N=19$ additional controls ($N=11$ H3K4me3, 4 female, 7 male; $N=17$ H3K27ac, 8 female, 9 male) passing ENCODE quality controls (>10 million uniquely mapped reads, normalized strand coefficient (NSC) > 1 and PCR bottleneck coefficient > 0.8; Supplementary Fig. 1 and Supplementary Table 2).

For downstream analysis, we consolidated multiple ChIP-seq datasets by cell type for each brain region and histone mark as (i) H3K4me3 PFC neuronal, (ii) H3K4me3 PFC neuron-depleted, (iii) H3K4me3 ACC neuronal, (iv) H3K4me3 ACC neuron-depleted, (v) H3K27ac PFC neuronal, (vi) H3K27ac PFC neuron-depleted, (vii) H3K27ac ACC neuronal and (viii) H3K27ac ACC neuron-depleted. Tissue homogenate samples for each histone mark were consolidated as (ix) H3K4me3 PFC HBCC homogenate and (x) H3K27ac PFC HBCC homogenate. (Although all our samples were acquired through the Human Brain Collection Core (HBCC) brain bank, the "HBCC" identifier was used for the homogenate samples alone in order to distinguish them from the Roadmap Epigenomics Project tissue homogenates in our subsequent analysis.) Supplementary Table 3 shows the list of samples in each of the ten consolidated datasets (see Methods for a detailed description of the consolidation steps). The average number of uniquely mapped and nonredundant reads for the consolidated datasets by cell type and brain region ranged from 13 to 41 million for H3K4me3 and 23 to 125 million for H3K27ac, reflecting that H3K27ac samples were sequenced at twice the coverage depth due to their larger width (Supplementary Fig. 1a). The subsequent steps of peak calling, read quantification of each peak, exploration of technical and biological covariates, differential modification analysis and functional annotation of peak sets (see Supplementary Fig. 2 for workflow diagram) were performed on each consolidated dataset. Across all individuals and both histone marks, ~50–70% of consolidated peaks in the cell-type-specific data and ~20–40% in the tissue homogenate data had read coverage of at least 1 count per million (CPM) (Supplementary Fig. 3).

To evaluate the specificity of our histone-modification maps, we compared the peak coordinates to published H3K4me3 and H3K27ac maps from the Roadmap Epigenomics Project (REP) covering 111 tissues[5]. The maximum similarity (estimated based on Jaccard's *J*) was found when our consolidated subset was compared to the REP brain tissues, while overlap with non-neural and peripheral REP tissues was lower (Supplementary Fig. 4 and Supplementary Table 4). For both brain regions and epigenetic marks, our neuron-depleted samples, which overwhelmingly comprise non-neuronal cells, had a higher similarity with REP brain samples than neuronal samples. Likewise, our NeuN$^-$ H3K27ac landscapes displayed a higher similarity with H3K27ac and also histone H3 acetyl-Lys9 (H3K9ac) landscapes collected from bulk cortex tissue (homogenate) from independent brain cohorts[10,11]. These observations, taken together, likely reflect the fact that the majority of cells residing in cortical gray matter are indeed non-neuronal[18].

Genome-wide analysis of H3K4me3 and H3K27ac peaks reveal cell type specificity. The cell-type-specific peak sets (peaks called on consolidated datasets i–viii above) varied by the fraction of the genome covered by peak regions, as well as by the degree of overlap with other subsets. As expected, the 61,000–95,000 narrow H3K4me3 peaks (range reflecting different cell types and cortical areas) covered a much smaller fraction of the genome than the 91,000–116,000 broader H3K27ac peaks (Supplementary Table 5). For example, in PFC neurons, H3K4me3 peaks covered 82 Mb (2.8%) of the genome, while H3K27ac covered 595 Mb (19.8%) in the same subset (Fig. 1b–e). Only minimal differences in the percentage of genomic coverage by H3K4me3 peaks (2.7–2.9%) was observed across cell types, whereas H3K27ac showed much higher genomic coverage for neuronal (19.8–20.4%) than neuron-depleted (15.5–16.9%) chromatin (Fig. 1c).

Principal component analysis revealed distinct clusters of neuronal, neuron-depleted (non-neuronal) and homogenate samples for both histone marks (Fig. 1f,g and Supplementary Fig. 5a); however, samples from the PFC and ACC clustered together (Supplementary Fig. 5b). This indicates a relatively high degree of epigenetic difference between neuronal and non-neuronal chromatin compared to a minimal difference between cortical areas. In contrast, chromatin from our PFC tissue homogenate samples and additional homogenate brain tissue from other sources[5,10] fell between that of the FACS-sorted cells along the first principal component (Fig. 1f,g). Notably, the HBCC homogenate PFC samples were much more similar to the non-neuronal component, and the fraction of NeuN$^-$ nuclei in our tissue homogenates comprised, on average, 60–70% of the total population (Supplementary Fig. 6 and Supplementary Table 6), which is consistent with the fact that non-neuronal cells outnumber neurons by 1.6–2:1 in the human frontal lobe[18]. To further explore this similarity of PFC homogenate with non-neuronal cells, we quantified and analyzed the non-overlapping regions of PFC neuronal, PFC neuron-depleted and PFC HBCC homogenate peak sets. PFC neuronal chromatin included vast amounts of H3K27ac (369 Mb) and H3K4me3 (46 Mb) peak sequences not shared with either neuron-depleted or tissue homogenate, while only 245 Mb (H3K27ac) and 15 Mb (H3K4me3) of peak sequences were unique to non-neuronal chromatin and not shared with tissue chromatin extracts or neurons (Fig. 2a). Taken together, these characteristics illustrate a crucial advantage of cell-specific data over homogenate data. Functional enrichment of genes in close proximity to these non-overlapping modified peak regions using GREAT[19] indicated distinct biological functions by cell type (Fig. 2b and Supplementary Table 7a–f). Neuron-specific H3K4me3 and H3K27ac peaks were enriched for ion channels, neurotransmitter signaling and synaptic genes, while genome regions marked in neuron-depleted and tissue homogenate peak sets showed enrichment for broader, less defined categories (Fig. 2b).

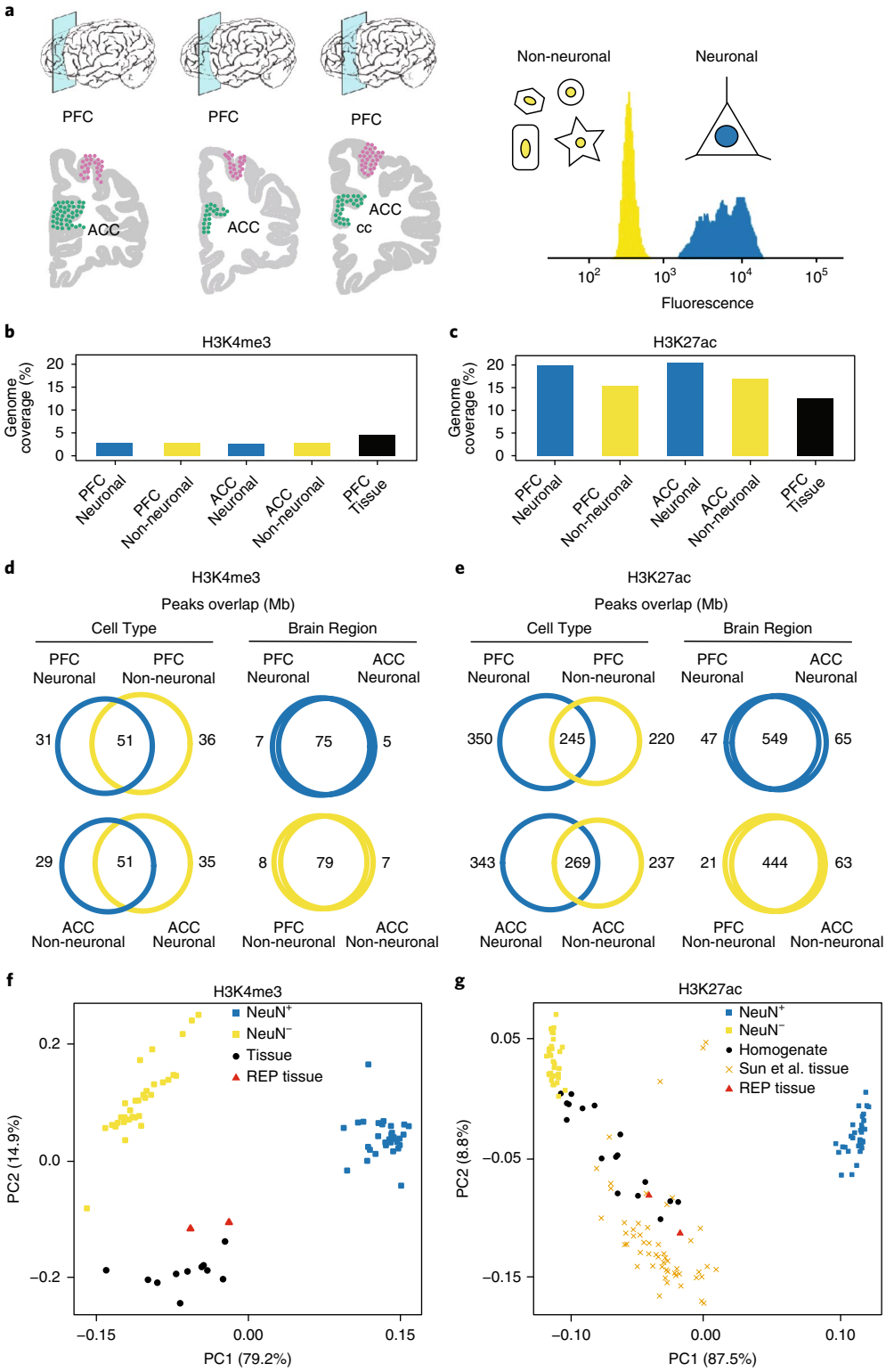

Fig. 1 | Cell- and region-specific histone modification profiling in the human frontal lobe. a, Left, regions of interest in dorsolateral PFC and ACC, positioned dorsal and anterior from rostral genu of corpus callosum (cc). Right, representative FACS nuclei sorting showing fluorescence of NeuN antibody binding separating nuclei into neuronal ($NeuN^+$) and neuron-depleted ($NeuN^-$) fractions. **b**,**c**, The genome-wide coverage of ChIP-seq peaks for each consolidated dataset: PFC neuronal, PFC neuron-depleted, ACC neuronal and ACC neuron-depleted, separately for H3K4me3 (**b**; *N* (brains) = 17 PFC $NeuN^+$, 14 ACC $NeuN^+$, 17 PFC $NeuN^-$, 15 ACC $NeuN^-$) and H3K27ac (**c**; *N* (brains) = 17 PFC $NeuN^+$, 17 ACC $NeuN^+$, 17 PFC $NeuN^-$, 15 ACC $NeuN^-$). **d**,**e**, Venn diagrams by histone mark (**d**, H3K4me3; **e**, H3K27ac), cell type (blue, neuronal; gold, neuron-depleted) and brain region, summarizing the overlap (expressed in megabases) of called peaks (MACS2, $P < 0.01$). **f**,**g**, Principal component analysis of pairwise correlations between each pair of ChIP-seq $\log_2$ counts per million of samples from each mark. Visualization of first two principal components (PCs), where data points are from (i) our cell-specific and homogenate dataset (PFC neurons and ACC neurons, blue squares; PFC non-neurons and ACC non-neurons, gold squares (*N* (samples) = 63 H3K4me3, 66 H3K27ac)); PFC homogenate, black circles (*N* (samples) = 11, H3K4me3; 17, H3K27ac)), (ii) the Roadmap Epigenomic Project (REP)[5] (ACC and PFC homogenate, red triangles), or (iii) Sun et al.[10] (PFC homogenate, orange crosses; *N* (brains) = 53, H3K27ac).

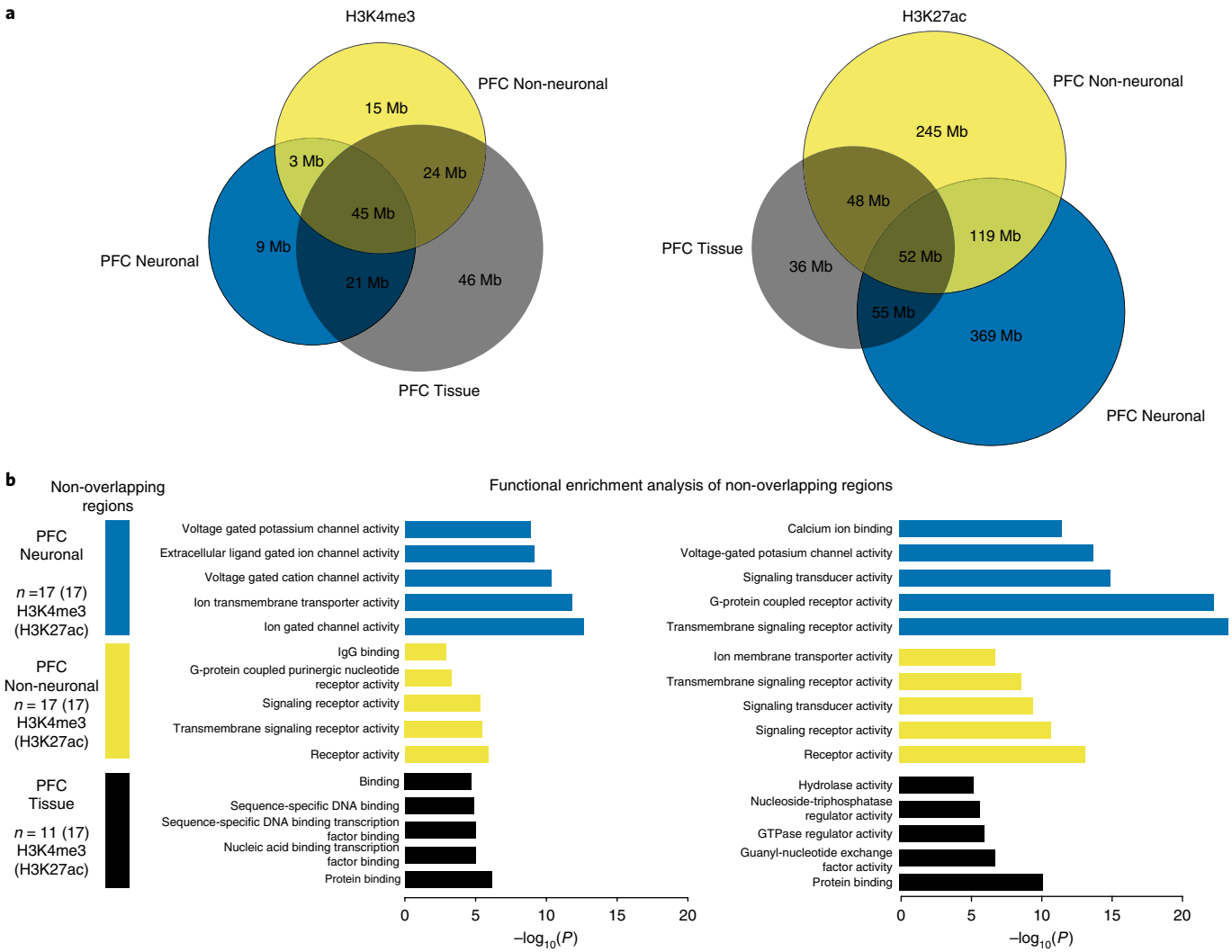

Fig. 2 | Functional enrichment of non-overlapping cell- and tissue-specific histone peaks. a, Venn diagrams showing overlap in megabases of peak regions between neuronal (blue), non-neuronal (gold) and homogenate (black) for H3K4me3 (left) and H3K27ac (right). **b**, Functional enrichments evaluated using GREAT[19] of peak regions that are unique to each of the three sets. Bar plots in blue, gold and black correspond to $-\log_{10}(P)$ from hypergeometric test of pathway enrichment results of peaks that are unique to neuronal, non-neuronal and homogenate, respectively. H3K4me3 *N* (brains) = 17 PFC NeuN$^+$, 17 PFC NeuN$^-$, 11 PFC tissue homogenate; H3K27ac *N* (brains) = 17 PFC NeuN$^+$, 17 PFC NeuN$^-$, 17 PFC tissue homogenate.

While this analysis has described large-scale trends, cell specificity of histone modification is readily visualized at the gene level. As representative examples, we consider *CAMK2A* and *OLIG1*, which are neuron- and non-neuron-specific genes, respectively (see Supplementary Fig. 7).

Collectively, our findings affirm that the neuronal epigenomic landscape is distinct from both non-neuronal and tissue homogenate landscapes. Although our findings indicate that chromatin maps from homogenate may omit critical neuron-specific epigenomic signatures, they do, however, provide a better representation of non-neuronal chromatin. Indeed, analysis of published brain hQTLs from H3K27ac profiles in cortical homogenate[10] showed modest enrichment for overlap with our NeuN$^-$ H3K27ac peaks, but a depletion for overlap with our NeuN$^+$ H3K27ac peaks (Supplementary Fig. 8). This enrichment was highly specific, as these hQTLs were depleted for overlap with H3K4me4 peaks. Moreover, analysis of another type of H3-acetyl mark, H3K9ac, from brain tissue homogenate[11] showed only depletion for overlap with the two marks from neuronal and neuron-depleted chromatin in this study (Supplementary Fig. 8).

Neuronal histone modification landscapes show strong enrichment of schizophrenia GWAS loci. Owing to the distinct histone modification landscapes between neuronal and non-neuronal cells in the frontal lobe, we wanted to better understand the role of cell- and region-specific epigenomic regulation associated with various psychiatric and nonpsychiatric traits. To this end, we used the linkage disequilibrium (LD)-score partitioned heritability method[20] to examine the enrichment of common genetic variants identified by genome-wide association studies (GWAS) within genomic regions with cell-type-specific histone modifications. Altogether, 18 different types of brain- and non-brain-related diseases and conditions were included in these analyses (Fig. 3).

The strongest enrichment was found for schizophrenia-associated loci; weaker (but nonetheless significant) enrichments were found for the genetic architectures associated with education years, intelligence, neuroticism, depressive symptoms, body mass index, chronotype and sleep duration (Supplementary Table 8a,b). Strikingly, each of these enrichments was almost exclusively limited to the neuronal histone modification landscapes of the PFC and ACC, suggesting that the aforementioned GWAS datasets link disease-associated vulnerabilities

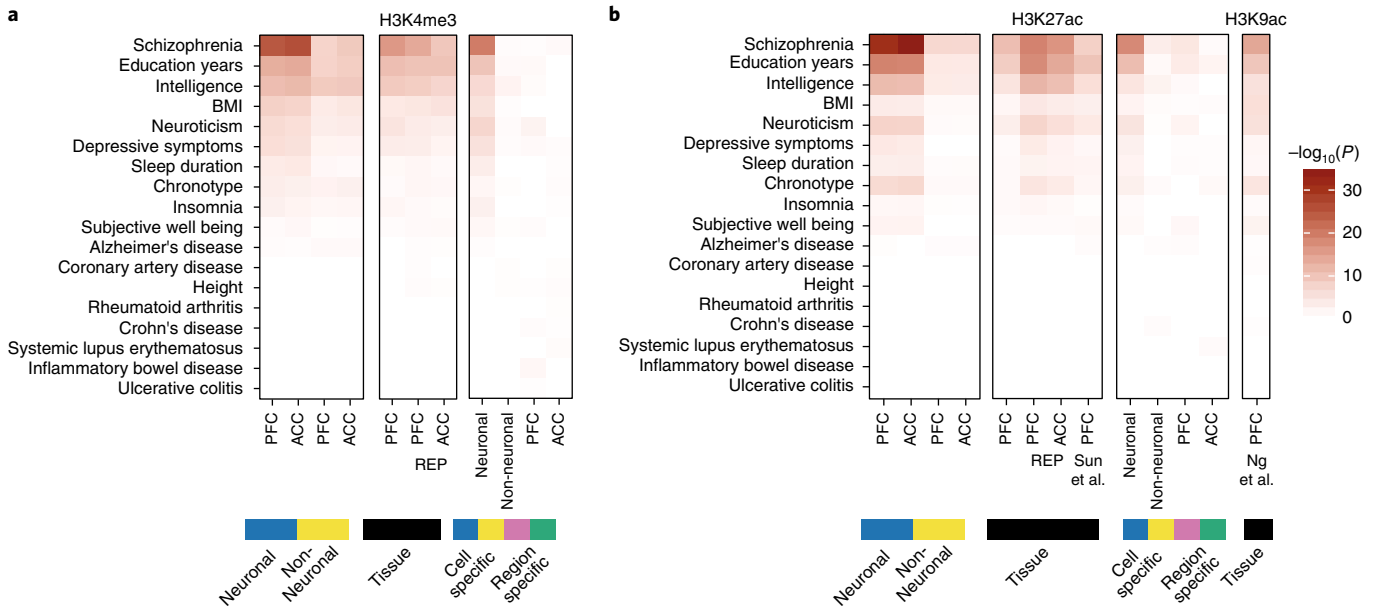

Fig. 3 | Enrichment of heritability for brain- and non-brain-related phenotypes within cell- and tissue-specific histone peaks. a,**b**, Using LD-score regression to partitioned heritability, we tested whether the genetic variants contributing to 18 brain- and non-brain-related phenotypes were enriched for H3K4me3 (**a**) and H3K27ac (**b**). In **a**, heritability enrichment analysis was performed on multiple sets of genome regions that are visualized in three blocks. (i) Regions marked in blue and gold show enrichment values of PFC neuronal (63,642 (105,075) peaks), ACC neuronal (61,043 (116,714) peaks), PFC neuron-depleted (95,501 (91,037) peaks) and ACC neuron-depleted (87,292 (101,885) peaks) from consolidated H3K4me3 (H3K27ac) datasets. (ii) Regions marked in black show enrichment value of PFC tissue from our dataset (158,345 (183,885) peaks), REP PFC tissue (75,912 (317,582) peaks), and REP ACC tissue (79,844 (260,288) peaks) for H3K4me3 (H3K27ac) marks. (iii) Regions showing statistically significant differential histone modification between either the two cell types or two brain regions. Results for peaks that show increased histone modification in neurons (28,838 (59,588) peaks) or non-neurons (31,790 (58,120) peaks) from H3K4me3 (H3K27ac) marks are indicated in blue and gold, respectively. Results for peaks that show increased histone modification in PFC (696 (10,665) peaks) or ACC (508 (10,797) peaks) from H3K4me3 (H3K27ac) are indicated in purple and green, respectively. Layout in **b** is the same as in **a** except that enrichment of 56,503 peaks from PFC tissue from Sun et al.[10] and 26,384 peaks from Ng et al.[11] are added. Regions marked in neurons consistently show the most significant enrichment for sequences associated with genetic risk for schizophrenia. H3K4me3 *N* (brains) = 17 PFC NeuN$^+$, 14 ACC NeuN$^+$, 17 PFC NeuN$^-$, 15 ACC NeuN$^-$, and 11 PFC tissue homogenate; H3K27ac *N* (brains) = 17 PFC NeuN$^+$, 17 ACC NeuN$^+$, 17 PFC NeuN$^-$, 15 ACC NeuN$^-$, 17 PFC tissue homogenate (HBCC). BMI, body mass index.

specifically to neurons. Indeed, the neuron-specific enrichment for sequences implicated in schizophrenia risk were consistently more significant than the comparatively weaker enrichment for these risk sequences in the histone modification maps from brain tissue homogenate herein, as well as in published H3K27ac[10] and H3K9ac[11] maps from brain tissue homogenate (Fig. 3 and Supplementary Fig. 9). For non-brain-related traits such as height, coronary artery disease, Crohn's disease and ulcerative colitis, we observed little enrichment for peaks from either neuronal and neuron-depleted chromatin. Furthermore, the strongest enrichment of brain related traits was identified in the non-overlapping peak regions of PFC neurons compared with the PFC HBCC homogenate peak sets, which further corroborates the association of GWAS loci of neuropsychiatric diseases with neuron-specific chromatin regions (Supplementary Fig. 9 and Supplementary Table 8c,d). Finally, LD-score regression coefficients[20] from the enrichment analysis of schizophrenia were significantly larger in neuronal as compared to neuron-depleted chromatin, and this effect was consistently observed for both histone marks in the two cortical regions, ACC and PFC (Supplementary Fig. 10). However, neither neuronal nor neuron-depleted PFC and ACC chromatin showed any significant overlap with Alzheimer's disease-associated variants, consistent with the hypothesis that Alzheimer's disease risk variants are enriched for regulatory sequences within cells of myeloid origin[21–23]

Decomposing quantitative variation in histone modification into multiple components. Quantitative epigenetic variation could be attributed to biological variation across cell types, subjects, brain regions and sexes. To quantify the percentage of variation in histone modification in each peak region that is attributable to each of these four variables plus residual variation, we fit a linear mixed model using variancePartition[24] (Fig. 4). Since variance percentages sum to 100%, these values can be easily compared across variables, peak regions and histone marks. The variance percentages are easily interpretable visually: a peak region with high variation across cell types shows distinct levels of histone modification in neuronal versus neuron-depleted chromatin (Fig. 4a). The genome-wide trend across all peak regions for each mark indicates that cell type was the strongest source of variation in histone modification, followed by subject (Fig. 4b,c). In contrast, variation across brain regions was very limited. Finally, as expected, variation across sexes was minimal genome-wide while exerting a strong effect on genes linked to chromosomes X and Y. To further clarify the extent to which epigenomic differences between male and female frontal cortex are driven by histone peaks located on the sex chromosomes, we conducted principal component analysis of our 83 H3K27ac samples (11 female, 72 male), including cell-type-specific and tissue homogenate datasets. Inclusion of regions on chromosomes X and Y indeed resulted in strong sex-specific clustering on the fourth principal component while male and female brains completely intermixed when the analyses with repeated under exclusion of histone-tagged sequences specific to the X and Y chromosomes (Supplementary Fig. 11).

Finally, to interpret the peak regions with the highest variation across subjects, we computed the overlap of peak regions from the current dataset with regions that have genome-wide significant

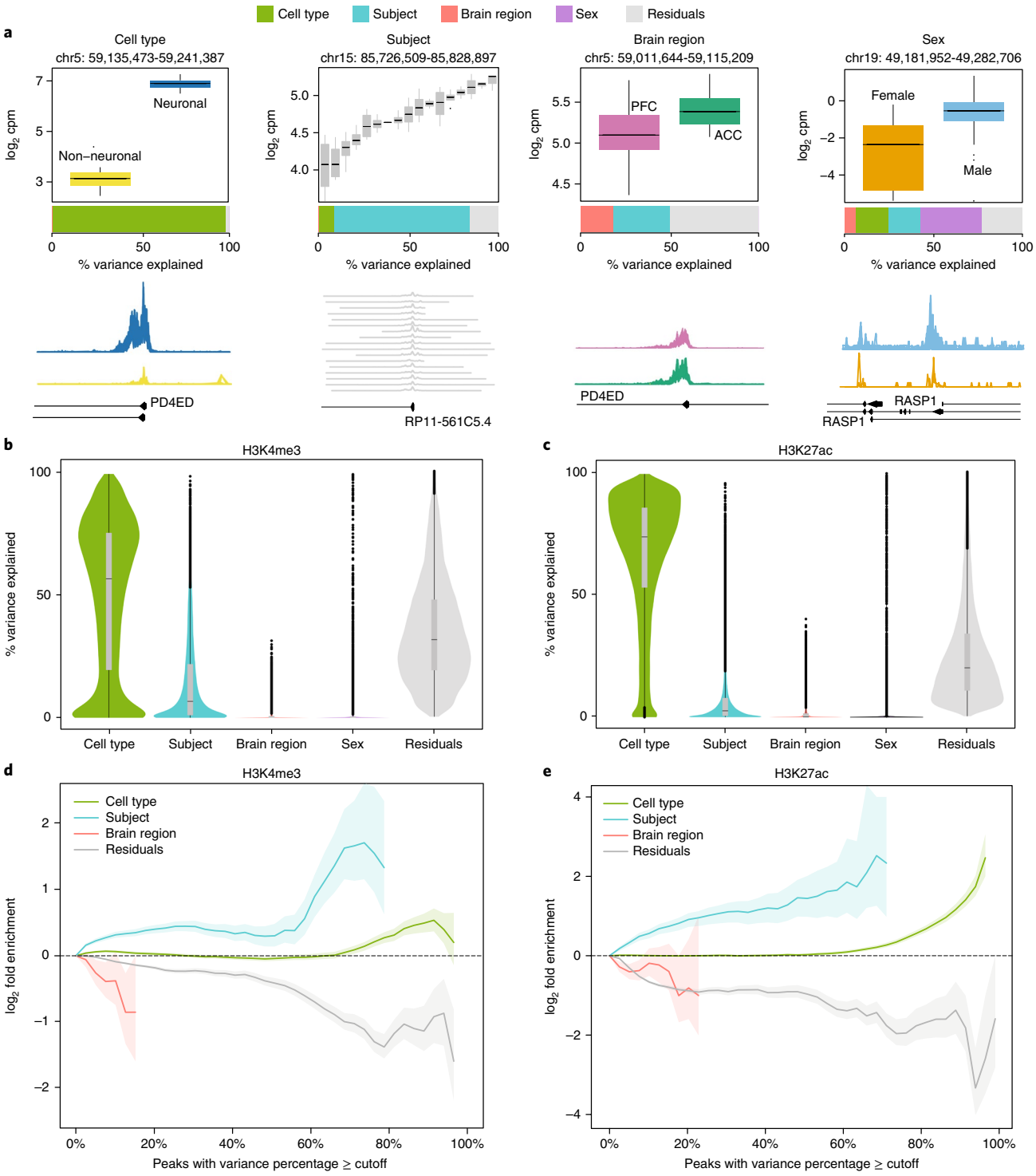

Fig. 4 | Decomposing multiples sources of epigenetic variation. The contribution of epigenetic variation across 2 cell types, 17 subjects, 2 brain regions and 2 sexes, plus residual variation, were quantified using a linear mixed model implemented in variancePartition. **a**, Representative examples of H3K4me3 consensus peaks (128,467 peaks from $n=63$ samples) wherein one source explains a large fraction of the epigenetic variation. Box plots indicate the $\log_2$ counts per million stratified by cell type, subject, brain region and sex. Box plot black horizontal line indicates median; box demarcates $\log_2$cpm in interquartile range (IQR) for a given peak region; vertical line above (below) the box plot show the 1.5IQR of the upper (lower) quartile. Bar plot below the box plot indicates the fraction of epigenetic variation in the peak explained by each variable. Genome coverage plot (bottom row) of ChIP-seq signal ($n=17$ individuals) from data subset PFC neuronal for each peak region shown in the box plot. **b**,**c**, Violin plots indicate the genome-wide distribution of epigenetic variation across the four variables, plus the residual variation for H3K4me3 (**b**; 128,467 peaks from $n=63$ samples) and H3K27ac (**c**; 147,539 peaks from $n=66$ samples). Each point represents a peak, and the width of the violin plot represents the number of peaks. Bar plot indicate the median and 25% and 75% quantiles. **d**,**e**, Fold enrichment of hQTLs identified in lymphoblastoid cell lines[25] and postmortem PFC[10] for peaks with variance explained by each variable exceeding the cutoff indicated on the *x* axis for H3K4me3 (**d**; $n=63$ samples) and H3K27ac (**e**; $n=66$ samples). Results for sex are not shown because enrichment for autosomal genes alone was considered. Shaded regions indicate 90% confidence interval from 10,000 permutations.

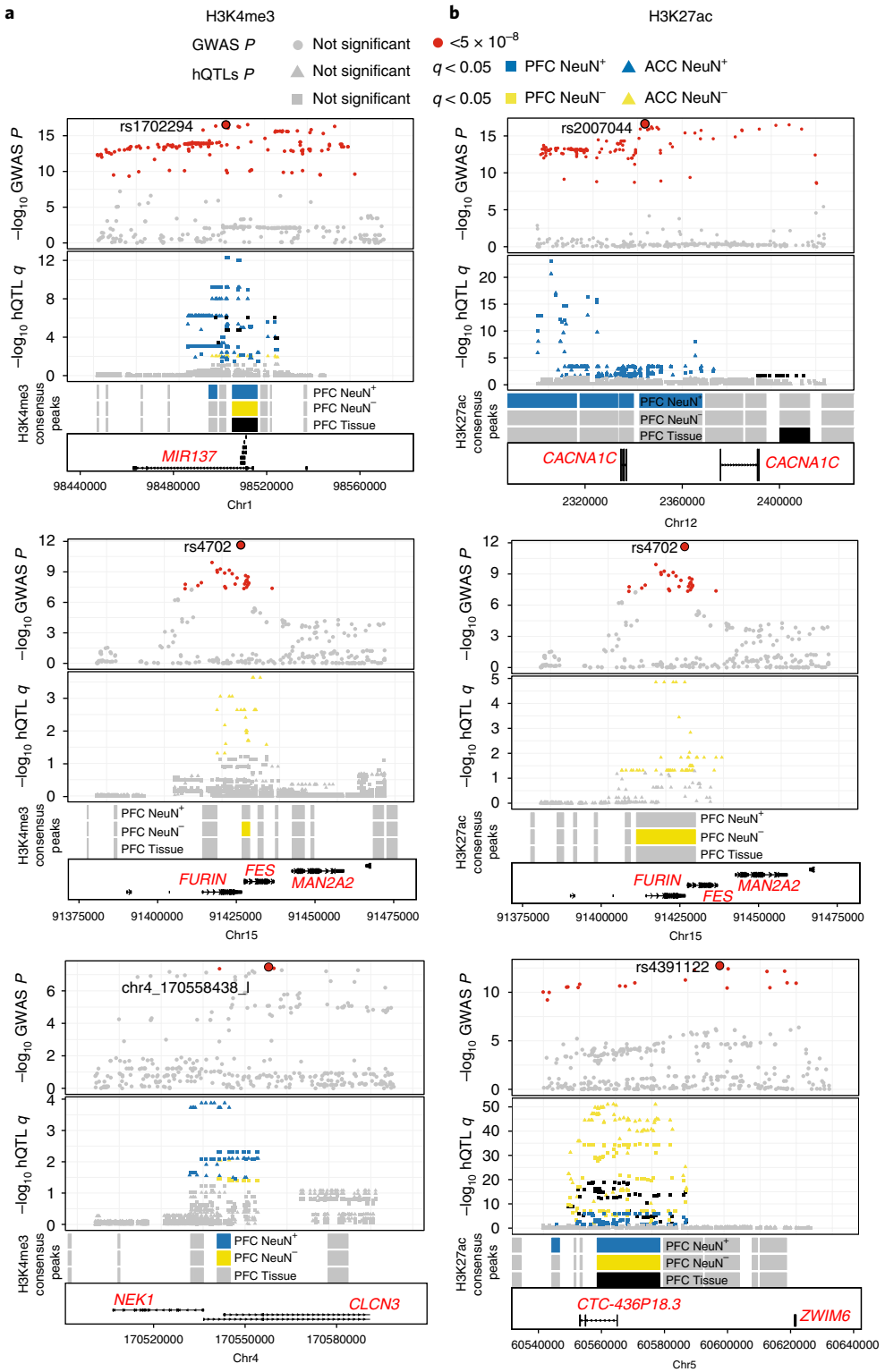

Fig. 5 | Overlap of cell-specific and homogenate hQTLs with genome-wide significant loci in schizophrenia. a,**b**, A few representative genome-wide significant loci in schizophrenia that overlap with cell-specific and homogenate hQTLs are shown. All significant SNPs ($P < 5 \times 10^{-8}$) are red, with the lead SNP a large red circle, and the rest are gray. Corresponding to these representative GWAS loci, overlapping cell-specific and homogenate hQTLs are shown in gray, with significant hQTLs (RASQUAL $q < 0.05$) blue (neurons), gold (non-neurons) and black (homogenate). Consensus peak regions for which hQTLs were called are shown in gray separately for neurons, non-neurons and homogenates. These tracks are colored blue, gold and black if they have any significant hQTL (RASQUAL $q < 0.05$) that overlaps with the representative genome-wide significant loci ($P < 5 \times 10^{-8}$). From top to bottom, loci shown are *MIR137*, *FURIN*, *CLCN3* for H3K4me3 (**a**) and *CACNA1C*, *FURIN* and *ZWIM6* for H3K427ac (**b**). H3K4me3 *N* (brains) = 17 PFC NeuN$^+$, 14 ACC NeuN$^+$, 17 PFC NeuN$^-$, 15 ACC NeuN$^-$, and 11 PFC tissue homogenate; H3K27ac *N* (brains) = 17 PFC NeuN$^+$, 17 ACC NeuN$^+$, 17 PFC NeuN$^-$, 15 ACC NeuN$^-$, 17 PFC tissue homogenate (HBCC).

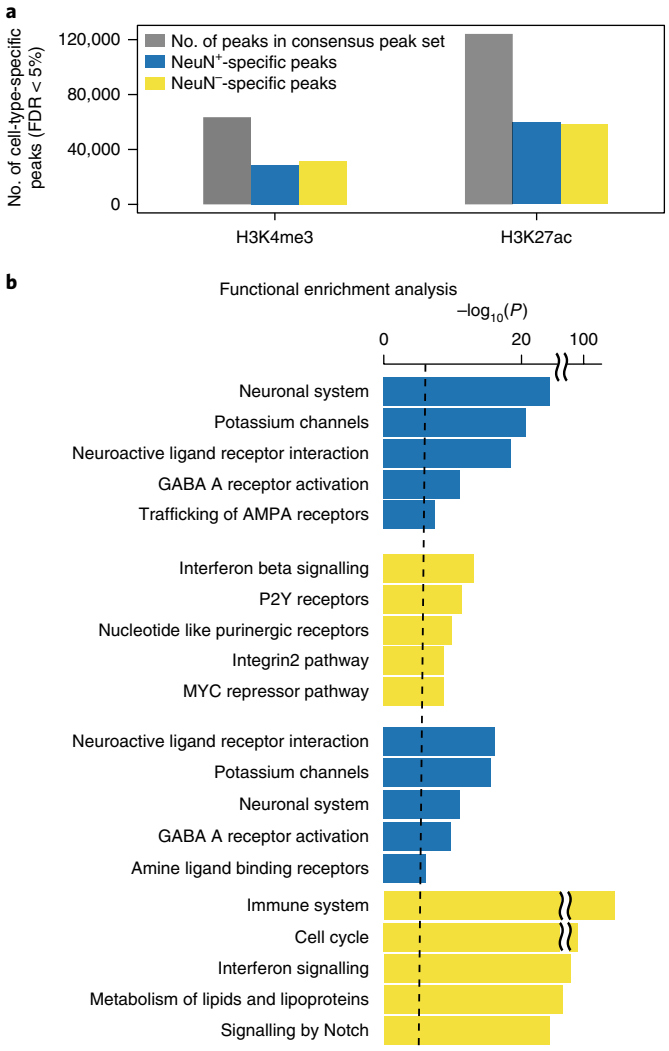

Fig. 6 | Regions differentially modified in neuronal and non-neuronal cell types. a, Bar plot of counts of differentially modified peaks for neuronal (blue) and neuron-depleted (gold) chromatin for H3K4me3 (top) and H3K27ac (bottom) at FDR < 5%. Differential modification analysis was performed on the normalized read count matrix with columns as genomic regions (128,467 (147,539)) and four types of samples (PFC neuronal, ACC neuronal, PFC neuron-depleted and ACC neuron-depleted from 17 individuals (brains)) as rows; *N* (samples) = 63 (66) after quality control for H3K4me3 (H3K27ac). **b**, Functional enrichments for genes near differentially modified peaks computed with GREAT. Bar plots corresponding to significant peaks (neuronal, 28,838 (59,588) and non-neuronal 31,790 (58,120) from H3K4me3 (H3K27ac) marks) identified in datasets from **a** (*N* (samples) = 63 (66) H3K4me3 (H3K27ac)) show top five pathways from REACTOME, Pathway Interaction Database and KEGG databases with $-\log_{10}(P)$ from hypergeometric test for neuronal and non-neuronal peaks. Dashed line shows the Bonferroni cutoff at 2×10^{-5}.

hQTLs identified in lymphoblastoid cell lines and human brains for the H3K4me3[25] and H3K27ac[10] epigenetic marks, respectively. Peak regions with high variation across subjects were indeed enriched for regions that are hQTLs in lymphoblastoid cell lines and human brains for their respective histone mark (Fig. 4d,e). This is consistent with variation in histone modification across subjects being driven at least in part by genetic regulatory variation[10,25,26]. Importantly, this enrichment is limited to loci subject to epigenomic regulation that are common between neuronal and neuron-depleted chromatin (this study) and tissue extract and lymphoblast lines from previous studies[10,25].

Genetic regulation of histone modification in neuronal and neuron-depleted fractions. To examine whether there is cell-type-specific genetic regulation of histone modifications (as has been observed previously for gene expression[6,27]), we applied RASQUAL (robust allele-specific quantitation and quality control), a QTL approach integrating allele-specific and between-subject differences[28]. Each of the four neuronal, neuron-depleted and bulk tissue chromatin preparations indeed harbored thousands of hQTLs, ranging from 6,695 to 8,042 for H3K27ac and 1,565 to 3,517 for H3K4me3 at a false discovery rate (FDR) < 0.05, depending on chromatin fraction (Supplementary Fig. 12 and Supplementary Table 9). Of note, H3K27ac-tagged chromatin showed unexpectedly strong enrichment for Gene Ontology GREAT biological processes such as neurofilament organization, regulation of synaptic plasticity, associative learning, catecholamine-dependent signaling and various other pathways highly relevant to the neurobiology of schizophrenia and other common psychiatric disease (Supplementary Fig. 13).

Since hQTLs calling was slightly underpowered as a result of the small sample size ($n = 36$), we took the simple approach of comparing our cell-specific and bulk tissue hQTLs with data from GWAS for schizophrenia[29]. We took all associations with $P < 5\times10^{-8}$ that are in high LD ($r^2 > 0.8$) with the lead single-nucleotide polymorphism (SNP) and evaluated their overlap with our hQTLs. Comparisons across bulk tissue, neuronal and neuron-depleted chromatin revealed strong cell-type-specific effects for many of these risk-associated loci. For example, H3K4me3 peaks near *MIR137* showed stronger hQTLs in neuronal samples than neuron-depleted and bulk tissue samples with localization of lead SNP rs1702294. H3K27ac peaks showed even stronger cell-specific hQTL signal near the voltage-gated calcium channel *CACNA1C* in neuronal samples, whereas peaks for both histone marks near *FURIN* showed a single hQTL only in neuron-depleted samples (Fig. 5, Supplementary Fig. 12 and Supplementary Table 10).

Epigenomic variation between ACC and PFC. Cell type was the major source of quantitative variation in histone modification, with 55,628 H3K4me3 and 117,708 H3K27ac peak regions epigenetically different across cell types at FDR 5% (Fig. 6a and Supplementary Fig. 14a). Unsurprisingly, for each histone mark, functional enrichment by gene categories was highly specific for cell type (Fig. 6b). However, differences in histone modification between ACC and PFC were much smaller because of the similarity between the brain regions. Differential histone modification analysis between brain regions in neuronal cells identified 508 H3K4me3 and 10,797 H3K27ac peaks with increased modification in ACC, as well as 696 H3K4me3 and 10,665 H3K27ac peaks in PFC (Supplementary Figs. 14b and 15a–c and Supplementary Tables 11 and 12). Notably, there was minimal region-specific signal in neuron-depleted chromatin, with only 27 H3K4me3 and 18 H3K27ac peaks with increased modification in ACC and none in PFC (Supplementary Fig. 15d). These results indicate dramatically higher regional specificity for the population of neurons compared to their surrounding non-neuronal cells in the frontal lobe. It remains to be determined whether the differential histone acetylation landscapes in PFC vs. ACC neurons are reflective of differences in neurocognitive function between these cortical areas. For example, there is robust ACC activation with regard to reward processing, pain, affect and emotion[30]. In contrast, dorsolateral PFC is frequently implicated in the regulation of goal-directed behavior, including working memory and executive functions[31]. We note that multiple peak regions that were differentially modified between PFC and ACC neurons are proximal to neuropsychiatric risk genes (Supplementary Tables 13 and 14). These include the forkhead transcription factor *FOXP1*, which functions synergistically with a related molecule, *FOXP2*, to regulate cognition and

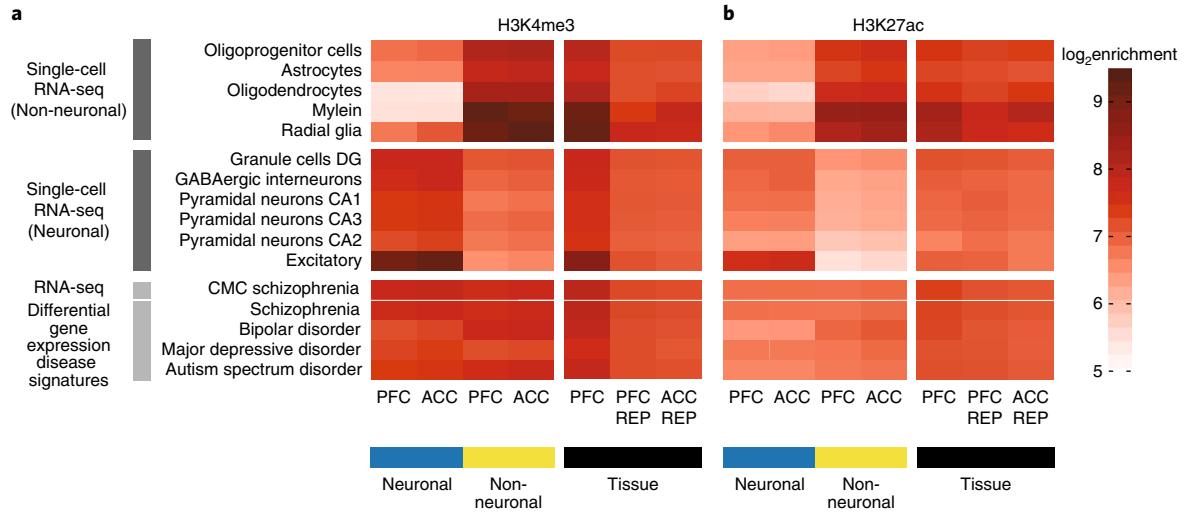

Fig. 7 | Cell-type-specific histone acetylation and methylation profiles are associated with differential enrichment for neuronal and glial transcripts. **a**,**b**, The colored tiles illustrates the $\log_2$ magnitude of enrichment of ChIP-seq counts (a, H3K4me3; b, H3K27ac) within 15 kb downstream and upstream of the TSS of gene sets that are identified with neuronal and non-neuronal cell types from (top) single-cell RNA sequencing[17] defining various neuronal and glial subtypes, as indicated, and (bottom) disease-associated gene expression profiles[36]. Enrichments were quantified for cell-specific datasets PFC and ACC neuronal (blue) and PFC and ACC neuron-depleted (gold), and for PFC tissue (homogenate) including HBCC and REP[5]. CMC, CommonMind Consortium; DG, dentate gyrus.

speech[32]; the exocytosis regulator *CADPS2*, which is essential for axonal release of brain-derived nerve growth factor (BDNF)[33]; and the *GRIK4* kainate receptor, relevant for a broad range of disorders on the autism, mood and psychosis spectrum[34,35].

Transcriptional signatures of promoter-bound histone methylation and acetylation. While histone peaks from neuronal and neuron-depleted chromatin were bound to promoters, introns and intergenic elements (Supplementary Fig. 16), annotation of the H3K4me3 and H3K27ac peak sequences in the consolidated subsets revealed that a large majority of sequences (70–79% of H3K4me3-tagged and 57–68% of H3K27ac-tagged) were bound to promoters within 5 kb of annotated transcription start sites (TSS). We therefore examined whether levels of H3K4me3 and H3K27ac modification are associated with gene expression magnitude in an independent set of postmortem brain samples from dorsolateral PFC from the CommonMind Consortium[7]. To this end, we calculated the number of ChIP-seq reads aligned within 15 kb of the annotated TSS of genes in five gene sets grouped by expression magnitude. As expected from findings in peripheral cells and tissues[8], both H3K4me3 and H3K27ac ChIP-seq reads were enriched around the TSS of genes with high levels of expression compared to genes with low levels of expression (Supplementary Fig. 17).

In our final analyses, we examined the association of the neuronal, neuron-depleted and homogenate chromatin landscape with gene expression magnitudes in multiple subtypes of neurons and glia recently identified by massively parallel profiling of single brain nuclei[17]. There were indeed strong cell-type-specific chromatin effects, with neuron-depleted chromatin showing strong enrichment for oligodendrocyte- and astrocyte-specific transcripts while conversely neuronal chromatin profiles were more strongly associated with transcripts of the various types of neurons as compared to glia (Fig. 7). In contrast, these enrichments showed no cell type specificity for chromatin fractions prepared from tissue homogenate (Fig. 7). Not limiting our analyses to cell types, we examined the association of neuronal, neuron-depleted and homogenate chromatin with differentially expressed transcripts in multiple cohorts of subjects diagnosed with autism, bipolar disorder or schizophrenia[36]. Both cell-type and homogenate chromatin fractions showed moderate levels of enrichment with these disease-related gene sets (Fig. 7).

Discussion

Interpreting the functional consequences of recently identified genetic variants contributing to the risk of neuropsychiatric disease requires a deeper understanding of the epigenomic context of these variants in brain and other tissues[2–4,6,10,11]. We built a dataset of cell-type-specific reference maps for NeuN$^+$ neuronal and NeuN$^-$ (overwhelmingly non-neuronal) histone modification landscapes for H3K4me3 and H3K27ac, which are typically associated with active promoter and enhancer regions, respectively. Notably, non-neuronal chromatin showed a high degree of concordance with epigenomic landscapes of cortical homogenates from multiple sources. In contrast, histone methylation and acetylation landscapes from ACC and PFC neurons showed considerable 'epigenomic distance' from neuron-depleted and tissue homogenate samples (Fig. 1f,g and Supplementary Fig. 5a), suggesting they are likely a poor surrogate for neuron-specific alterations in the context of cognitive function and neurological disease. Given that the differences between neuronal and non-neuronal H3K4me3 and H3K27ac landscapes are the major axis of epigenomic variation (Fig. 4), it will be essential for future studies to pursue more sample fractionation by cell type in order to capture the estimated 16 neuronal populations defined by single-cell RNA sequencing in human cerebral cortex[37], as well as potentially similar degrees of heterogeneity in glia, as recently reported for mouse brain[38]. Such a higher resolution approach is expected to reveal vast numbers of genomic loci with an epigenomic signature unique to a specific type of neuron or glia, and provide deeper insight into the interrelation of transcriptome and histone modification landscapes. We also note the unexpectedly large quantitative H3K27ac differences between cell types, with a much larger genome coverage (20%) in neuronal chromatin decorated by histone acetylation versus only 15–16% genome coverage in neuron-depleted chromatin. The extended H3K27ac coverage broadly included intronic and intergenic sequences, in addition to many promoter-bound peaks (Supplementary Fig. 16). While the functional implications of the extended H3K27ac peak coverage in the neuronal genome remains to be explored, we note

that drugs interfering with the regulation of histone acetylation, including histone deacetylase inhibitors and suppressors of histone acetylation reader proteins, show a surprisingly broad therapeutic profile, improving cognition and neuronal function in a wide range of neuropsychiatric disease models[39–41]. Furthermore, consistent with previous gene expression profiles in adult frontal cortex[42], the transcriptional histone marks of the present study, H3K4me3 and H3K27ac, showed few sex-specific histone methylation and acetylation differences in the autosomal genome (Supplementary Fig. 11). However, previous DNA methylation profiling in cortical tissue homogenate from aged brains revealed sex-specific effects for approximately 10% of age-sensitive methyl-CpG marks[43]. At present, it is not known whether sex-specific regulation of histone modifications is increased in the aged brain.

One primary goal of the PsychENCODE Consortium is to explore regulatory noncoding DNA associated within the genetic risk architectures of common neuropsychiatric disorders[6]. Using LD-score regression to partition heritability[20], we found strong, specific enrichments for schizophrenia and somewhat weaker association with depression, neuroticism and education attainment in both H3K4me3 and H3K27ac peaks (Fig. 3). This effect was primarily if not exclusively driven by neuronal chromatin (Fig. 3 and Supplementary Figs. 9 and 10), with minimal or no contribution from neuron-depleted chromatin. Intriguingly, the strongest association with brain-region-specific peaks identifies risk variants for schizophrenia and educational attainment specifically in PFC neurons, consistent with the key role of the PFC in executive function. Taken together, these findings underscore the importance of epigenomic fine mapping with maximal region- and cell-type-specific resolution for the human brain in order to link the genetic risk architectures of neuropsychiatric disorders to selected cell populations or neural circuits.

Our cell-type-specific reference maps, accessible through the PsychENCODE Knowledge Portal and UCSC browser on Synapse (https://www.synapse.org/#!Synapse:syn4566010), are a resource that will empower future studies exploring the epigenetic foundations of cell-type-specific genome organization and function in human brain, with important implications for the neurobiology of common psychiatric disease.

Methods

Methods, including statements of data availability and any associated accession codes and references, are available at https://doi.org/10.1038/s41593-018-0187-0.

Received: 15 December 2017; Accepted: 25 May 2018;
Published online: 23 July 2018

References

1. Geschwind, D. H. & Flint, J. Genetics and genomics of psychiatric disease. *Science* **349**, 1489–1494 (2015).
2. Gandal, M. J., Leppa, V., Won, H., Parikshak, N. N. & Geschwind, D. H. The road to precision psychiatry: translating genetics into disease mechanisms. *Nat. Neurosci.* **19**, 1397–1407 (2016).
3. Bernstein, B. E. et al. The NIH Roadmap Epigenomics Mapping Consortium. *Nat. Biotechnol.* **28**, 1045–1048 (2010).
4. Farh, K. K.-H. et al. Genetic and epigenetic fine mapping of causal autoimmune disease variants. *Nature* **518**, 337–343 (2015).
5. Kundaje, A. et al. Integrative analysis of 111 reference human epigenomes. *Nature* **518**, 317–330 (2015).
6. Akbarian, S. et al. The PsychENCODE project. *Nat. Neurosci.* **18**, 1707–1712 (2015).
7. Fromer, M. et al. Gene expression elucidates functional impact of polygenic risk for schizophrenia. *Nat. Neurosci.* **19**, 1442–1453 (2016).
8. Zhou, V. W., Goren, A. & Bernstein, B. E. Charting histone modifications and the functional organization of mammalian genomes. *Nat. Rev. Genet.* **12**, 7–18 (2011).
9. Network and Pathway Analysis Subgroup of Psychiatric Genomics Consortium. Psychiatric genome-wide association study analyses implicate neuronal, immune and histone pathways. *Nat. Neurosci.* **18**, 199–209 (2015).
10. Sun, W. et al. Histone acetylome-wide association study of autism spectrum disorder. *Cell* **167**, 1385–1397.e1311 (2016).
11. Ng, B. et al. An xQTL map integrates the genetic architecture of the human brain's transcriptome and epigenome. *Nat. Neurosci.* **20**, 1418–1426 (2017).
12. Cheung, I. et al. Developmental regulation and individual differences of neuronal H3K4me3 epigenomes in the prefrontal cortex. *Proc. Natl. Acad. Sci. USA* **107**, 8824–8829 (2010).
13. Shulha, H. P., Cheung, I., Guo, Y., Akbarian, S. & Weng, Z. Coordinated cell type-specific epigenetic remodeling in prefrontal cortex begins before birth and continues into early adulthood. *PLoS Genet.* **9**, e1003433 (2013).
14. Charney, D. S., Sklar, P. B., Buxbaum, J. D. & Nestler, E. J. *Charney & Nestler's Neurobiology of Mental Illness* (Oxford Univ. Press, New York, 2018).
15. Mancarci, B. O. et al. Cross-laboratory analysis of brain cell type transcriptomes with applications to interpretation of bulk tissue data. *eNeuro* **4**, ENEURO.0212-17.2017 (2017).
16. Huttner, H. B. et al. The age and genomic integrity of neurons after cortical stroke in humans. *Nat. Neurosci.* **17**, 801–803 (2014).
17. Habib, N. et al. Div-Seq: single-nucleus RNA-Seq reveals dynamics of rare adult newborn neurons. *Science* **353**, 925–928 (2016).
18. Sherwood, C. C. et al. Evolution of increased glia-neuron ratios in the human frontal cortex. *Proc. Natl. Acad. Sci. USA* **103**, 13606–13611 (2006).
19. McLean, C. Y. et al. GREAT improves functional interpretation of cis-regulatory regions. *Nat. Biotechnol.* **28**, 495–501 (2010).
20. Finucane, H. K. et al. Partitioning heritability by functional annotation using genome-wide association summary statistics. *Nat. Genet.* **47**, 1228–1235 (2015).
21. Huang, K. L. et al. A common haplotype lowers PU.1 expression in myeloid cells and delays onset of Alzheimer's disease. *Nat. Neurosci.* **20**, 1052–1061 (2017).
22. Gjoneska, E. et al. Conserved epigenomic signals in mice and humans reveal immune basis of Alzheimer's disease. *Nature* **518**, 365–369 (2015).
23. Raj, T. et al. Polarization of the effects of autoimmune and neurodegenerative risk alleles in leukocytes. *Science* **344**, 519–523 (2014).
24. Hoffman, G. E. & Schadt, E. E. variancePartition: interpreting drivers of variation in complex gene expression studies. *BMC Bioinformatics* **17**, 483 (2016).
25. Grubert, F. et al. Genetic control of chromatin states in humans involves local and distal chromosomal interactions. *Cell* **162**, 1051–1065 (2015).
26. Waszak, S. M. et al. Population variation and genetic control of modular chromatin architecture in humans. *Cell* **162**, 1039–1050 (2015).
27. GTEx Consortium. The Genotype-Tissue Expression (GTEx) pilot analysis: multitissue gene regulation in humans. *Science* **348**, 648–660 (2015).
28. Kumasaka, N., Knights, A. J. & Gaffney, D. J. Fine-mapping cellular QTLs with RASQUAL and ATAC-seq. *Nat. Genet.* **48**, 206–213 (2016).
29. Schizophrenia Working Group of the Psychiatric Genomics Consortium. Biological insights from 108 schizophrenia-associated genetic loci. *Nature* **511**, 421–427 (2014).
30. Posner, M. I., Rothbart, M. K., Sheese, B. E. & Tang, Y. The anterior cingulate gyrus and the mechanism of self-regulation. *Cogn. Affect. Behav. Neurosci.* **7**, 391–395 (2007).
31. Moghaddam,B . & Homayoun,H . Divergent plasticity of prefrontal cortex networks. *Neuropsychopharmacology.* **33**, 42–55 (2008).
32. Le Fevre, A. K. et al. FOXP1 mutations cause intellectual disability and a recognizable phenotype. *Am. J. Med. Genet. A* **161A**, 3166–3175 (2013).
33. Sadakata, T. et al. Reduced axonal localization of a Caps2 splice variant impairs axonal release of BDNF and causes autistic-like behavior in mice. *Proc. Natl. Acad. Sci. USA* **109**, 21104–21109 (2012).
34. Griswold, A. J. et al. Evaluation of copy number variations reveals novel candidate genes in autism spectrum disorder-associated pathways. *Hum. Mol. Genet.* **21**, 3513–3523 (2012).
35. Kawaguchi, D. M. & Glatt, S. J. GRIK4 polymorphism and its association with antidepressant response in depressed patients: a meta-analysis. *Pharmacogenomics* **15**, 1451–1459 (2014).
36. Gandal, M. J. et al. Shared molecular neuropathology across major psychiatric disorders parallels polygenic overlap. *Science* **359**, 693–697 (2018).
37. Lake, B. B. et al. Neuronal subtypes and diversity revealed by single-nucleus RNA sequencing of the human brain. *Science* **352**, 1586–1590 (2016).
38. Zeisel, A. et al. Molecular architecture of the mouse nervous system. Preprint at bioRxiv https://doi.org/10.1101/294918 (2018).
39. Sullivan, J. M. et al. Autism-like syndrome is induced by pharmacological suppression of BET proteins in young mice. *J. Exp. Med.* **212**, 1771–1781 (2015).
40. Penney, J. & Tsai, L. H. Histone deacetylases in memory and cognition. *Sci. Signal.* **7**, re12 (2014).
41. Jakovcevski, M. & Akbarian, S. Epigenetic mechanisms in neurological disease. *Nat. Med.* **18**, 1194–1204 (2012).
42. Kang, H. J. et al. Spatio-temporal transcriptome of the human brain. *Nature* **478**, 483–489 (2011).
43. Yang, J. et al. Association of DNA methylation in the brain with age in older persons is confounded by common neuropathologies. *Int. J. Biochem. Cell Biol.* **67**, 58–64 (2015).

Acknowledgements

We thank M. Fromer, E. Stahl, L. Huckins, L. Shen, G. Senthil and T. Lehner for discussion. This paper is dedicated to the memory of Pamela Sklar. This work was supported in part through the computational resources and staff expertise provided by Scientific Computing at the Icahn School of Medicine at Mount Sinai. We are extremely grateful to J. Ochando, C. Bare and other personnel of the Icahn School of Medicine at Mount Sinai's Flow Cytometry Core for providing and teaching cell sorting expertise. Data were generated as part of the PsychENCODE Consortium, supported by U01MH103339, U01MH103365, U01MH103392, U01MH103340, U01MH103346, R01MH105472, R01MH094714, R01MH105898, R21MH102791, R21MH105881, R21MH103877 and P50MH106934 awarded to S.A. (Icahn School of Medicine at Mount Sinai), G. Crawford (Duke), S. Dracheva (Icahn School of Medicine at Mount Sinai), P. Farnham (USC), M. Gerstein (Yale), D. Geschwind (UCLA), T. M. Hyde (LIBD), A. Jaffe (LIBD), J. A. Knowles (USC), C. Liu (UIC), D. Pinto (Icahn School of Medicine at Mount Sinai), N. Sestan (Yale), P.S. (Icahn School of Medicine at Mount Sinai), M. State (UCSF), P. Sullivan (UNC), F. Vaccarino (Yale), S. Weissman (Yale), K. White (UChicago) and P. Zandi (JHU). Data were generated as part of the CommonMind Consortium supported by funding from Takeda Pharmaceuticals Company Limited, F. Hoffman-La Roche Ltd and NIH grants R01MH085542, R01MH093725, P50MH066392, P50MH080405, R01MH097276, RO1-MH-075916, P50M096891, P50MH084053S1, R37MH057881, R37MH057881S1, HHSN271201300031C, AG02219, AG05138 and MH06692. Brain tissue for the study was obtained from the following brain bank collections: the Mount Sinai NIH Brain and Tissue Repository, the University of Pennsylvania Alzheimer's Disease Core Center, the University of Pittsburgh NeuroBioBank and Brain and Tissue Repositories and the NIMH Human Brain Collection Core. CMC Leadership: P.S., J. Buxbaum (Icahn School of Medicine at Mount Sinai), B. Devlin, D. Lewis (University of Pittsburgh), R. Gur, C.-G. Hahn (University of Pennsylvania), K. Hirai, H. Toyoshiba (Takeda Pharmaceuticals Company Limited), E. Domenici, L. Essioux (F. Hoffman-La Roche Ltd), L. Mangravite, M.A.P. (Sage Bionetworks), T. Lehner and B.K.L. (NIMH). Data on coronary artery disease and myocardial infarction have been contributed by CARDIoGRAMplusC4D investigators. We also thank the International Genomics of Alzheimer's Project (IGAP) for providing summary results data for these analyses. The investigators within IGAP contributed to the design and implementation of IGAP and/or provided data but did not participate in analysis or writing of this report. IGAP was made possible by the generous participation of the control subjects, the patients, and their families. The i–Select chips were funded by the French National Foundation on Alzheimer's disease and related disorders. EADI was supported by the LABEX (Laboratory of Excellence Program Investment for the Future) DISTALZ grant, Inserm, Institut Pasteur de Lille, Université de Lille 2 and the Lille University Hospital. GERAD was supported by the Medical Research Council (grant no. 503480), Alzheimer's Research UK (grant no. 503176), the Wellcome Trust (grant no. 082604/2/07/Z) and German Federal Ministry of Education and Research (BMBF): Competence Network Dementia (CND) grant no. 01GI0102, 01GI0711, 01GI0420. CHARGE was partly supported by NIH NIA grant R01 AG033193 and NIA AG081220 and AGES contract N01–AG–12100, NHLBI grant R01 HL105756, the Icelandic Heart Association, and the Erasmus Medical Center and Erasmus University. ADGC was supported by NIH NIA grants U01 AG032984, U24 AG021886 and U01 AG016976, and Alzheimer's Association grant ADGC–10–196728.

Author contributions

Wet lab work including tissue processing, sorting of nuclei and ChIP-seq library generation: Y.J., L.B., M.K., E.Z., R.J., J.R.W., R.P., B.S.K. Data processing and coordination: Y.J., M.K., D.H.K., J.S.J., L.S., S.K.S., M.A.P., Y.-c.W., H.S. Bioinformatics and computational genomics: K.G., G.E.H., M.E.H., N.J.F., E.M., Z.W. Provision of brain tissue and resources: B.T.H., B.K.L. Conception of study design (including wet lab and/or bioinformatic analyses pipelines): Y.J., K.G., G.E.H., P.R., P.S., S.A. Writing of the paper: K.G., G.E.H., P.S., P.R., S.A.

Competing interests

The authors declare no competing financial interests.

Additional information

Supplementary information is available for this paper at https://doi.org/10.1038/s41593-018-0187-0.

Reprints and permissions information is available at www.nature.com/reprints.

Correspondence and requests for materials should be addressed to G.E.H. or P.R. or S.A.

Publisher's note: Springer Nature remains neutral with regard to jurisdictional claims in published maps and institutional affiliations.